

Recon3D enables a three-dimensional view of gene variation in human metabolism

Elizabeth Brunk^{1,2} , Swagatika Sahoo^{3,11}, Daniel C Zielinski¹, Ali Altunkaya^{4,5} , Andreas Dräger⁶ , Nathan Mih¹, Francesco Gatto^{1,7} , Avlant Nilsson⁷ , German Andres Preciat Gonzalez³ , Maike Kathrin Aurich³, Andreas Prlic⁴, Anand Sastry¹, Anna D Danielsdottir³, Almut Heinken³, Alberto Noronha³, Peter W Rose⁴, Stephen K Burley^{4,8}, Ronan M T Fleming^{3,9} , Jens Nielsen^{2,7} , Ines Thiele³  & Bernhard O Palsson^{1,2,10} 

Genome-scale network reconstructions have helped uncover the molecular basis of metabolism. Here we present Recon3D, a computational resource that includes three-dimensional (3D) metabolite and protein structure data and enables integrated analyses of metabolic functions in humans. We use Recon3D to functionally characterize mutations associated with disease, and identify metabolic response signatures that are caused by exposure to certain drugs. Recon3D represents the most comprehensive human metabolic network model to date, accounting for 3,288 open reading frames (representing 17% of functionally annotated human genes), 13,543 metabolic reactions involving 4,140 unique metabolites, and 12,890 protein structures. These data provide a unique resource for investigating molecular mechanisms of human metabolism. Recon3D is available at <http://vmh.life>.

It is widely recognized that progress in the biomedical sciences is hampered by the difficulty of integrating multiple disparate data types to obtain a coherent understanding of physiology and disease¹. A genome-scale network reconstruction represents a curated knowledge-base containing many different data types and sources, including high-quality genome annotation, assessment of biochemical properties of gene products, and a wide array of physiological functional information. Computational genome-scale models integrate large-scale omics data from these knowledge-bases to aid in the interpretation and prediction of biological functions². In recent years, human metabolic network reconstructions^{3–6} have generated insights into inborn errors of metabolism⁷, cancer⁸, and human microbiome co-metabolism^{9,10}.

Using metabolic reconstructions, researchers store and continually update information about chemical reactions in a standardized biochemical and genetic representation¹¹. Over the past ten years, updating the human metabolic network reconstruction has focused on expanding metabolic reaction coverage. From the first human reconstruction, Recon1 (ref. 4), to the most recent version, Recon2 (ref. 3), the content has been expanded from 1,496 genes (corresponding to 3,311 reactions) to 1,675 genes (7,785 reactions). Various other reconstructions have been released and community-driven efforts have been made to ensure interoperability of these resources^{3,5}.

Historically, systems biology has focused on characterizing the catalytic or regulatory roles of proteins in metabolism without placing

emphasis on the 3D structure of the proteins themselves. For example, studies on genetic variation have mainly focused on frequency of occurrence¹² or sequence-based attributes¹³. Only recently have mutations been explored in the context of their 3D location or spatial relationship to each other^{14–17}. Exploring mutations in 3D extends beyond nucleotide sequence identity¹⁸, as mutations that may be far away from each other in linear sequence may be proximal in the folded state. The availability of protein and metabolite structure data have enabled the progression of systems biology to a 3D perspective. In one study, protein structures were mapped to the metabolic network of *Escherichia coli*, to reveal the role of ribosome pausing in co-translational protein folding¹⁹. In another, human population variation was studied by integrating protein structures with the human erythrocyte metabolic network to understand the adverse effects of drugs on genetic variants²⁰ and identify new pathways related to drug perturbation. These studies highlight the value of integrating different types of data to address complex biological questions.

We present Recon3D, an updated and expanded human metabolic network reconstruction that integrates pharmacogenomic associations, large-scale phenotypic data, and structural information for both proteins and metabolites. Recon3D contains over 6,000 more reactions than Recon2, all of which were manually curated to remove redundant or blocked reactions. We use Recon3D to prioritize putative disease-causing genetic variants by mapping single-nucleotide

¹Department of Bioengineering, University of California, San Diego, San Diego, California, USA. ²The Novo Nordisk Foundation Center for Biosustainability, Technical University of Denmark, Lyngby, Denmark. ³Luxembourg Centre for Systems Biomedicine, University of Luxembourg, Campus Belval, Esch-Sur-Alzette, Luxembourg. ⁴RCSB Protein Data Bank, San Diego Supercomputer Center, University of California, San Diego, La Jolla, California, USA. ⁵Department of Computer Science, Arizona State University, Tempe, AZ 85281, Arizona, USA. ⁶Applied Bioinformatics Group, Center for Bioinformatics Tübingen (ZBIT), University of Tübingen, Tübingen, Germany. ⁷Department of Biology and Biological Engineering, Chalmers University of Technology, Gothenburg, Sweden. ⁸Department of Chemistry and Chemical Biology, Center for Integrative Proteomics Research, Institute for Quantitative Biomedicine, and Rutgers Cancer Institute of New Jersey, Rutgers, The State University of New Jersey, Piscataway, New Jersey, USA. ⁹Division of Analytical Biosciences, Leiden Academic Centre for Drug Research, Faculty of Science, University of Leiden, Leiden, the Netherlands. ¹⁰Department of Pediatrics, University of California, San Diego, La Jolla, CA, USA. ¹¹Present address: Department of Chemical Engineering, Indian Institute of Technology, Madras, India. Correspondence should be addressed to I.T. (ines.thiele@gmail.com) or B.O.P. (palsson@eng.ucsd.edu).

Received 19 June 2016; accepted 10 January 2018; published online 19 February 2018; doi:10.1038/nbt.4072

variants (SNVs) to protein structures. We show that deleterious mutations are more likely to cluster together into functional hotspots than non-deleterious mutations. In contrast to previous models, these mutation hotspots identify *ACAT1* as a cancer-related gene. Furthermore, we demonstrate how structural information can be used to investigate the potential mechanisms by which drugs exert an effect on metabolism. Recon3D provides new avenues for investigating the molecular basis of disease and may aid the development of treatment strategies, biomarkers, and drug repurposing.

RESULTS

Increasing the scope of the human metabolic network

We expanded Recon 2 (ref. 3) by using ten metabolomic data sets to identify new metabolites and transport and catalyzing reactions (1,865 reactions). We added reactions from HMR 2.0 (ref. 21) (2,478), a drug module²² (721), a transport module²³ (51), host–microbe reactions¹⁰ (24), and absorption and metabolism of dietary compounds (20). Overall, 66 metabolic subsystems, including lipoprotein (44 reactions) and bile acid (216 reactions), were expanded and 10 new subsystems were added (**Supplementary Figs. 1–3, Supplementary Data 1 and 2, and Supplementary Note 1**). We further refined numerous aspects of the reconstruction, including 2,181 gene–protein–reaction (GPR) associations, reaction/metabolite duplication, reaction directionality, and thermodynamic feasibility (Online Methods). The metabolic scope was extended by 82% for reactions (total 13,543) and 58% for unique metabolites (total 4,140) (**Fig. 1a,b**). Recon3D is the most comprehensive metabolic resource currently available (**Supplementary Table 1a–c**). Out of the 20,266 human proteins documented in UniProt²⁴ (queried July 2016), 19,213 are functionally annotated (i.e., not hypothetical) and 17% of this subset is metabolic, well-characterized, and included in Recon3D.

Genome-scale network reconstructions can be converted into computational models that enable predictive biology². We derived a computational model from Recon3D by removing reactions that were stoichiometrically inconsistent and that were flux inconsistent (i.e., reactions that could not carry flux under the applied reaction bounds; **Supplementary Note 2** and **Supplementary Data 1**). After performing standard quality-control tests, the resulting generic Recon3D model contained 10,600 reactions (78% of the reconstruction reactions) and was able to reproduce literature-consistent energy (ATP) yields from different carbon sources (**Supplementary Data 3–10**), to fulfill metabolic functions describing cellular and whole body metabolism, and to replicate the predictions of infant growth from a previous study²⁵ (**Supplementary Fig. 4**).

Enabling a 3D view of metabolism

Using a recently established approach²⁶, the metabolic network content of Recon3D was expanded to include 3D protein structures from the Protein Data Bank (PDB)²⁷ as well as homology models (**Fig. 2a**, **Supplementary Fig. 5** and **Supplementary Data 11–13**). In addition, we mapped content from a variety of external database resources, to include metabolite structures (**Supplementary Data 14**). We obtained high-quality structural coverage for over 80% of the human metabolic proteome (**Fig. 2a**, **Supplementary Fig. 6** and **Supplementary Tables 2–4**) and 85% of the metabolome (**Fig. 2b**). Furthermore, we used 2,369 unique metabolite structures to algorithmically trace atom transitions²⁸ (from each substrate to product atom) for 7,804 (87%) internal, mass-balanced reactions of the Recon3D-derived model (**Supplementary Note 3**). The prediction accuracy of the algorithms was validated by comparison with 512 manually curated atom-mapped reactions (**Fig. 2c** and **Supplementary Fig. 7**). The atom mappings

enable identification of conserved moieties, which are the fundamental structural units of any chemical reaction network. Hence, we provide an invaluable bridge between metabolic modeling and chemoinformatics. For the first time, relationships between human metabolic genes, their encoded proteins, and the reactions they catalyze can be described in the context of specific 3D configurations, interactions, and properties (**Fig. 1c,d**).

Web visualization of protein structures in metabolic networks

Using Recon3D, we have implemented the first web-based visualization of 3D macromolecular structures in the context of their neighboring chemical reactions, metabolites, and their metabolic subsystems (e.g., glycolysis, citric acid cycle, amino acid metabolism, and carbohydrate metabolism, among others). This tool utilizes a recently developed global human network map²⁹, together with network visualization software and conversion tools (**Supplementary Note 4** and **Supplementary Figs. 8–11**) and is available through the RCSB PDB website (<http://www.rcsb.org/>). The systems biology interface provides users with the ability to visualize networks that have been annotated to highlight which reactions are associated with experimental crystallographic structures, homology models, or metabolite structures (**Fig. 2d**). Dataframes for Recon3D are found in the github repository (<https://github.com/SBRG/Recon3D>).

Gene variation in 3D

We probed mutations in the context of representative protein domains (i.e., common structural regions redundant across the proteome). Such domains (e.g., tim-barrel motif) are often linked directly to their encoding gene's function, and thus provide a new way to directly assess the functional impact of a mutation.

We used Recon3D to map missense mutations from the Single Nucleotide Polymorphism database (dbSNP)³⁰, UniProt²⁴, and PharmGKB³¹, among others, to the metabolic network, using a previously established pipeline²⁰ (**Fig. 3a**). We chose to focus on SNPs that were known to be deleterious or potentially harmful. In total, we mapped 3,536 SNPs to 655 genes within Recon3D. We identified representative protein domains for this set of genes using a structure-based clustering algorithm³². We tallied the number of SNPs (or SNVs) occurring in each protein domain and found the gene-to-domain ratio to be <1 (i.e., domain redundancy; **Supplementary Fig. 12a**). This analysis resulted in the identification of specific regions within protein domains that are commonly mutated (mutation hotspots), share common disease associations, and are prone to malfunction. Six genes share the Bruton's tyrosine kinase representative domain (PDP:4RFZa, PF007714) and, when mutated, are affiliated with diseases such as cancer (**Fig. 3b**). This kinase domain is known for its role in non-small-cell lung cancer³³, and the SNPs associated with lung cancer cluster in one specific region of the protein (see the red-colored mutation hotspot in **Fig. 3b**).

The power of exploring gene variation in the context of both protein and network structure is further illustrated by Aryl sulfatase A (ARSA). Within the subset of SNPs that map to the representative domain of ARSA (SCOP: d1e2sp_), the mutation P428L (P426L in PDB 1e2s; dbSNP rs28940893) is associated with metachromatic leukodystrophy disease (MLD)³⁴. This mutation influences the biological assembly of ARSA, in which the native homo-octamer state (**Fig. 4a**) is disfavored relative to the dimeric state (**Fig. 4b**). Other SNPs associated with the most severe form of MLD are located in the vicinity of the metal binding site, a mutation hotspot (**Fig. 4c**). ARSA is also located within a 'network hotspot', with other deleterious SNPs dispersed throughout the neighborhood of surrounding reactions (**Fig. 4d**).

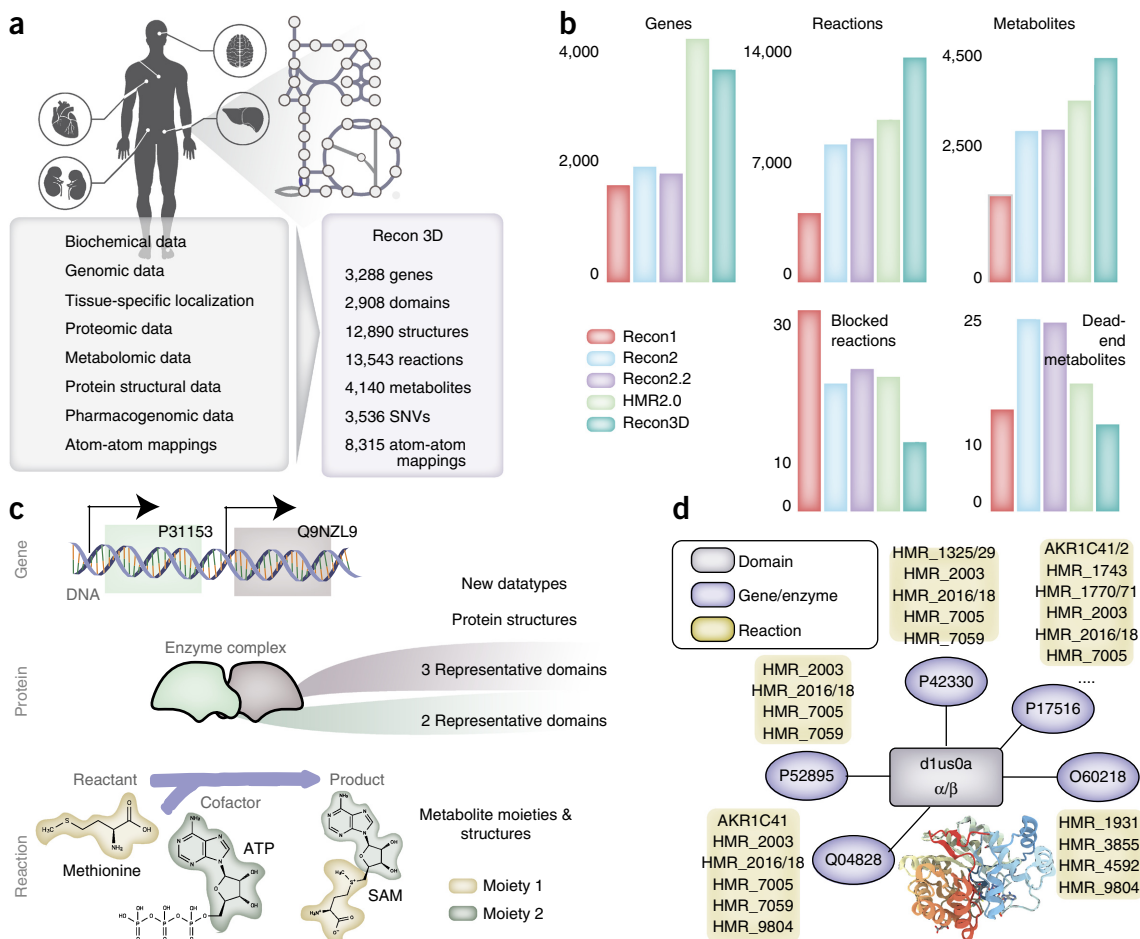


Figure 1 The properties and content of the Recon3D knowledge-base. **(a)** Recon3D includes information on 3,288 open reading frames that encode metabolic enzymes catalyzing 13,543 reactions on 4,140 unique metabolites, protein structural information from Protein Data Bank (PDB)²⁷, and metabolite structures from CHEBI⁵². It is capable of performing flux-balance analysis to integrate and interpret a variety of emerging data types, including linking mutations identified from human variation data or cancer genome atlases. **(b)** A comparison of the genes, reactions, metabolites, blocked reactions, and dead-end metabolites among Recon predecessors^{3–5} and HMR2.0 (ref. 6). **(c)** Relationships between genes, the proteins they encode, and the reactions the proteins catalyze (i.e., GPRs) are now described in the context of their specific 3D configurations, interactions, and properties. New data types include representative structural domains³² of proteins, metabolite structures along with their conserved moieties, and atom-atom mappings. Atom-level transitions were analyzed for 8,315 reactions (Supplementary Note 3). **(d)** Domain connectivity explored across the network to identify domains that are shared across multiple proteins, or involved in multiple catalyzing reactions. An example is the alpha/beta protein domain (d1us0a_{α/β}), which is present in eight different genes (described by Uniprot accession number). The proteins encoded by these genes belong to the reductase family; they catalyze different reactions in various metabolic subsystems, ranging from glycolysis and the pentose phosphate pathway to xenobiotics metabolism and glycerophospholipid metabolism. Recon3D can be queried and downloaded from <http://bigg.ucsd.edu/> or <http://vmh.life/>. Users can visualize protein structures in networks via <http://www.rscb.org> or visualize network simulation results using the interactive ReconMap built on the Google Maps API (<http://vmh.life/#mapnavigator>).

All mappings between SNPs, PDB, their representative domain, hotspots, and disease relevance are provided in Supplementary Data 15–20.

Oncogenic mutations cluster in structurally equivalent positions in the human proteome

The first application of Recon3D demonstrates its capability to discriminate pathogenic mutations from passenger mutations. We studied 889 somatic cancer mutations in 86 genes (which were previously analyzed³⁵) from whole-exome sequence data of 178 tumor–normal pairs of lung squamous cell carcinoma³⁶. Furthermore, we obtained detailed annotations about each of the mutations from cBioPortal³⁷, including whether a gene is a known oncogene^{37,38} or the mutation is recurrent¹², has a gain-of-function (GOF) mutation, and has a drug

association. Using Recon3D, we mapped each of the mutations to its corresponding protein, and the protein's representative domain(s) and network reaction(s) (Fig. 5a).

Analysis of all cancer mutations in the context of their representative protein domains suggests that oncogenic mutations cluster in structurally equivalent positions within representative domains. For the 86 genes, we counted the number of mutations that occur within 5 Å of another mutation within the representative domain (referred to as the 3D hotspot analysis; Online Methods and Supplementary Note 5). In some cases, mutations from different genes co-occurred in the same region of a shared domain, suggesting that the shared domain plays an important role in oncogenesis. Mutations co-occurring in the same location as other mutations are significantly more likely to be associated with somatic mutations, when compared to a random selection ($P < 0.02$,

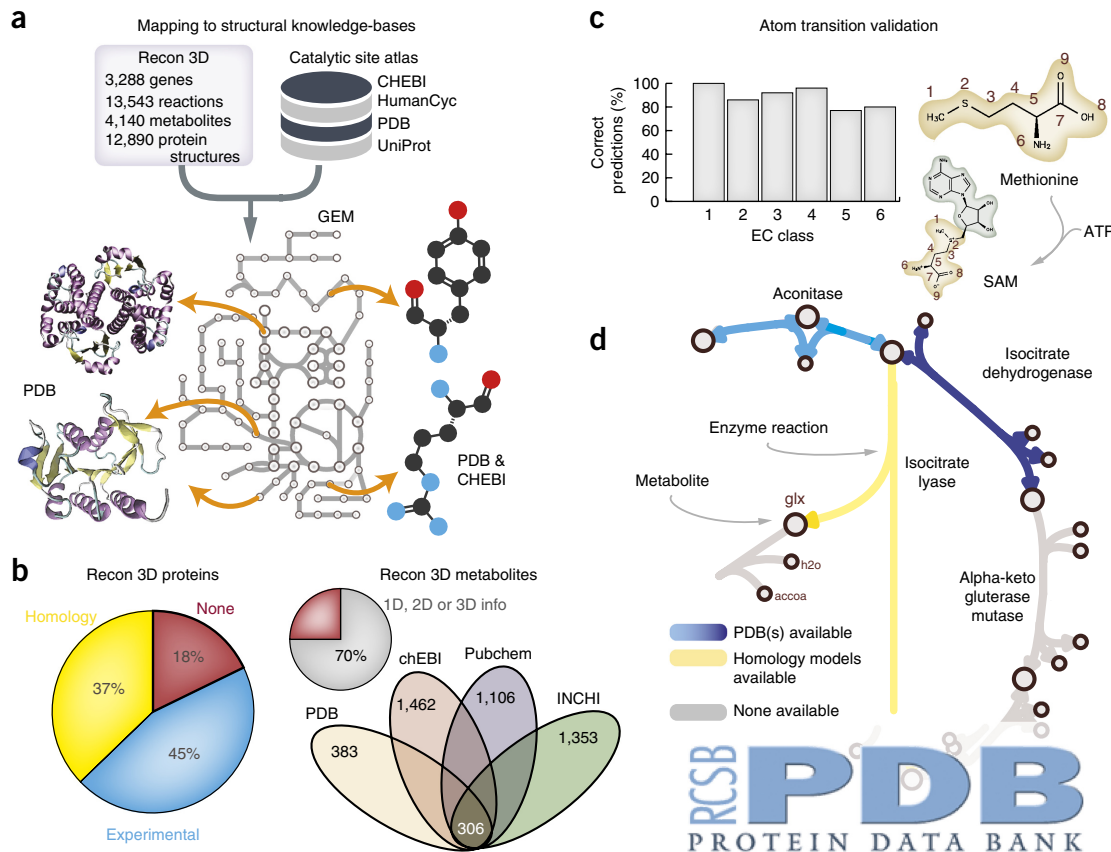


Figure 2 Linking the human metabolic network to protein structural databases, cheminformatics platforms, and the Protein Data Bank. (a) The metabolic content in Recon3D was cross-referenced with sequence and structure-based databases, such as UniProt²⁴ and PDB²⁷. The links in the metabolic network, which represent reactions, were mapped to 3D structures through their encoding genes. The nodes in the network, which represent metabolites, were also linked to structural representations (3D, 2D, or 1D connectivity specifications). (b) Structural coverage of both proteins and metabolites in Recon3D is given by the pie charts, which indicate that over 80% of the metabolic proteome (2,793/3,297 genes) and 85% of the unique metabolome (2369/2797) has structural information. In the case of metabolite structures, the combination of structural data from multiple sources allows for the total structural coverage to exceed 70%. (c) Validation of atom–atom mapping by comparison with curated atom mappings for each major class of reaction. Recon3D is the first metabolic network reconstruction to contain atomic-level details. (d) An example of the type of visualization that can be found at the RCSB PDB website: <http://www.rcsb.org/>. The systems biology interface provides users with the ability to visualize metabolic network maps, that have been annotated to highlight which reactions are associated with experimental crystallographic structures (blue), homology models (yellow), or metabolite structures.

using a two-tailed *t*-test; Fig. 5b). All data mapping related to the somatic cancer mutations can be found in Supplementary Data 21–23.

Filtering mutations based on their spatial relationships brings about several significant biomedical implications. When mutations are rank-ordered by the number of neighboring mutations, we can filter the mutations with known roles in oncogenesis (based on known annotations³⁷; Fig. 5c). For example, we find that selecting the top 25% of data by this ranking recovers 82% and 88% of known oncogenic mutations and GOF mutations (based on analysis via co-occurrence aids), respectively (compared with only 1.6% of oncogenic mutations and 2.9% of GOF mutations when selected at random; Fig. 5c; for a sensitivity analysis, see Supplementary Note 5). Furthermore, striking similarities in protein structure, based on 3D structure alignments, indicate that not only do mutations co-occur in shared domains, they also occur in structurally similar proteins within the same data set (Supplementary Fig. 12b). These findings suggest that cancer mutations cluster in functionally relevant parts of protein domains and that this property could guide the discovery of novel biomarkers and drug targets.

We combined our approach with metabolic modeling to understand whether structural information could improve the predictive power of

the model. We focused on glioblastoma multiforme (GBM), a malignant brain tumor, and studied the mutational landscape of metabolic genes (Fig. 5a). Genes were selected based on the rate of mutation found in exome samples of 291 glioblastomas as well as involvement in cholesterol metabolism³⁹ (Supplementary Note 5). Gene knockdowns were performed and the essential genes were compared across different generic and cell-type-specific human metabolic models (Recon3D, HMR2, and HMR-derived and TCGA-derived models⁸). Notably, the majority of models predicted the gene ACAT1 (GeneID 38) to be non-essential (Fig. 5d and Supplementary Fig. 13). Yet, a 3D hotspot analysis of the mutations in this gene suggested that it may be important in cancer (Fig. 5e). This finding was recently validated, confirming that inhibition of ACAT1 suppresses GBM growth by blocking SREBP-1-mediated lipogenesis⁴⁰. This result highlights the potential for structure-based analysis in genome-scale models to identify important genes for cell growth.

Co-occurring mutations across shared protein domains are significantly more deleterious

We used Recon3D to identify potentially deleterious mutations in a large-scale population study. We analyzed SNP data from multiple

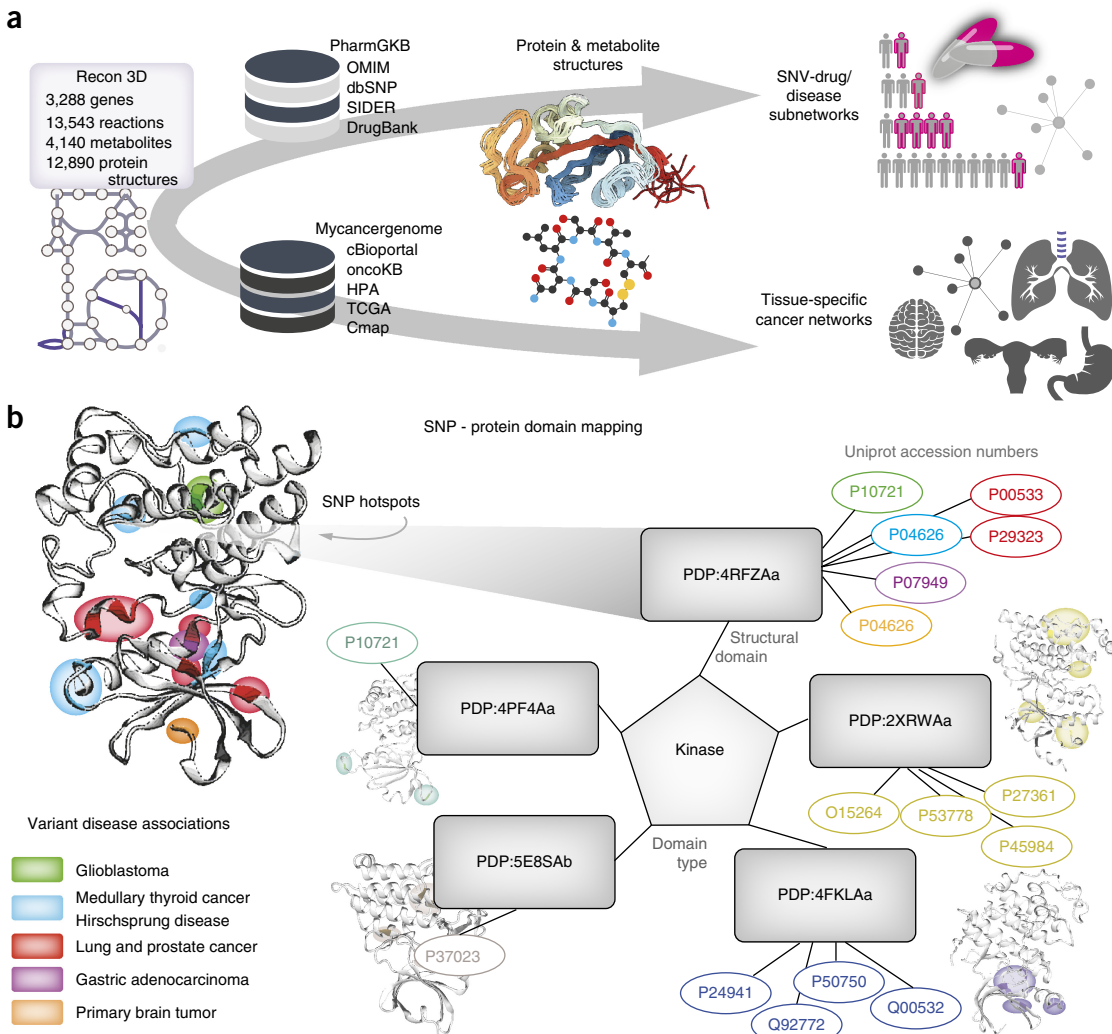


Figure 3 Linking the human metabolic network to gene variation and cancer knowledge-bases. (a) Recon3D, as a resource, provides information on three important layers of data related to disease biology: (i) amino acid location of mutations (or SNVs and SNPs) in the set of metabolic genes; (ii) the 3D structure of proteins with sequence variants; and (iii) the relationships between mutations and the onset of disease. Information was cross-referenced from Recon3D to human variation and pharmacogenomics databases, such as dbSNP³⁰, PharmGKB³¹, and cancer-specific databases, such as TCGA, the Human Protein Atlas (HPA), and CMap. We mapped SNVs and SNPs to the genes in Recon3D. Within the set of genes with genetic variation, we focused on cases where (1) protein structural data were available; (2) SNPs/SNVs were considered to be deleterious or potentially harmful (655 genes). (b) Using this information, we probed characteristics of missense mutations and their 3D spatial relationships. For each protein, we identified its representative protein structural domain (or a fold or set of folds unique to a given protein or multiple proteins). For example, for kinases, we identify various representative domains (five are shown here) that are associated with one or multiple genes (given by UniProt accession numbers). To this end, these five representative domains constitute “structure-based protein templates” shared among a group of genes. As illustrated, numerous mutations are found in 3D localized “hotspots” (or regions of the domain that experience high mutation burden). Interestingly, these mutation hotspots appear to be associated with specific diseases, such as primary brain cancer, glioblastoma, and other cancers in the case of Bruton’s tyrosine kinase (BTK) kinase domain scaffold (PDP:4RFZAA). All domains are determined by structural alignment³² and those featured here are named by the Protein Domain Parser (PDP) and the corresponding PDB structure (and chain) selected as the representative domain (**Supplementary Note 3**). Colors map genes to the region (hotspot) of their respective variant(s) and the diseases associated with that variant.

gene variation databases (dbSNP³⁰, UniProt²⁴, and PharmGKB³¹) and assessed whether the 3D location of variants in a gene could, in general, discern whether mutations were deleterious or tolerated⁴¹. We mapped over 10,000 SNPs to their 3D structural coordinates using our 3D hotspot analysis workflow and computed the number of mutations co-occurring in 5- and 10-Å spheres in common protein domains. 1,385 unique genes had 3,649 SNPs that mapped to regions of a protein where structural data exist. We computed the number of mutational co-occurrences across this set of SNPs and found that deleterious mutations are much more likely to neighbor other deleterious mutations ($P < 0.05$ using a

two-tailed t -test) than those predicted to be tolerated ($P > 0.1$, using a two-tailed t -test; **Supplementary Fig. 14** and **Supplementary Tables 5** and **6**). These added features enable predictive power over any existing model, in that mutational data can be assessed in the context of protein structure and compared with network-level, genome-wide model knockdowns (e.g., **Fig. 5e**). Prior reconstructions are unable to identify structural changes that affect complex assembly or other intrinsic protein properties. Such details can now be explicitly studied using Recon3D. To this end, Recon3D provides new inroads for metabolic models to explore disease-relevant mutations.

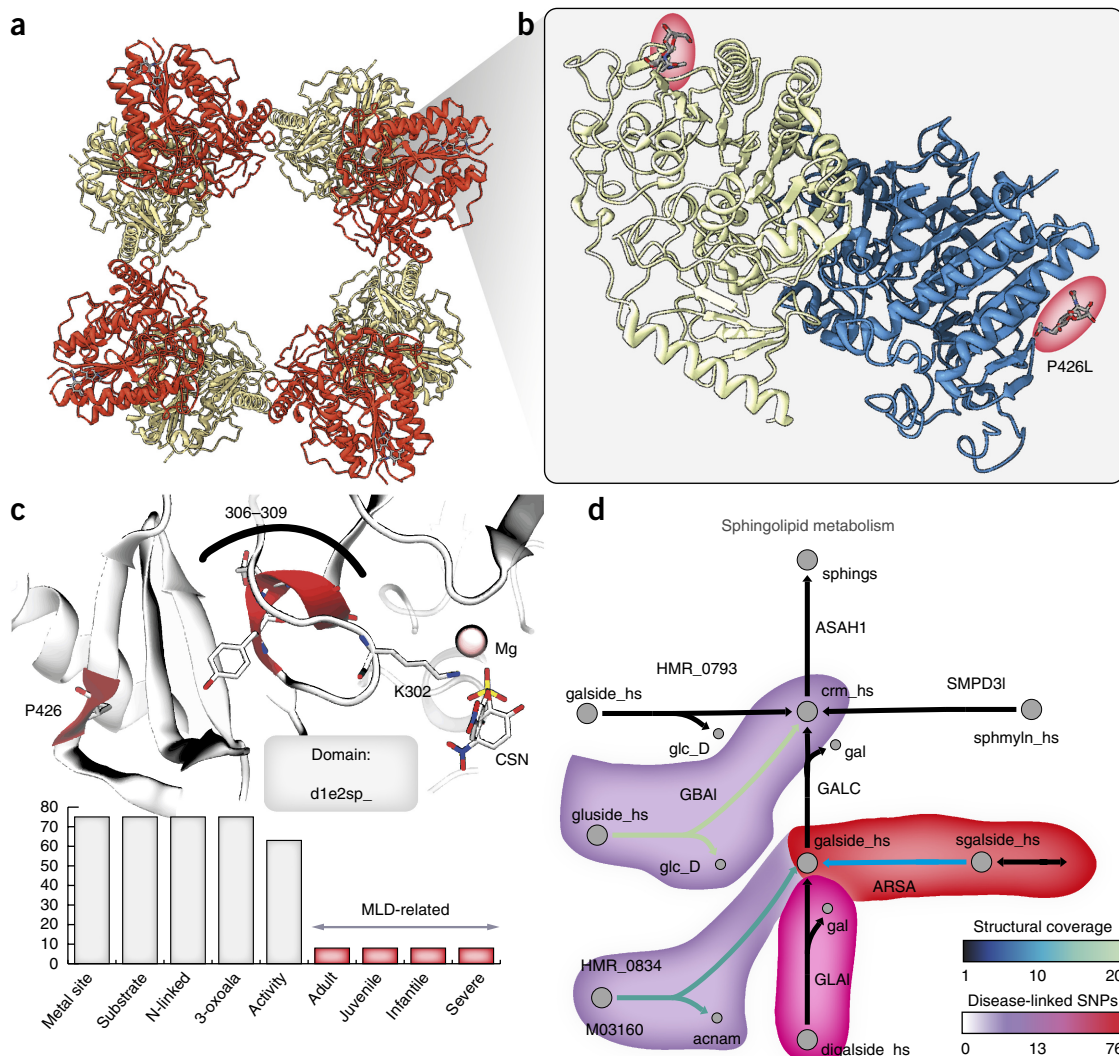


Figure 4 An example of bridging systems biology and structural biology through Recon3D. **(a)** Arylsulfatase A (ARSA) highlights an example of how the intersection of systems, and structural and pharmacogenomic information provides additional understanding of human disease variants. The macromolecular assembly in the native state contains a homo-octamer (four complexes of homodimers; PDB entry 1auk). **(b)** Identifying the location of a variant (e.g., P426L, dbSNP rs28940893) within the protein 3D structure reveals mechanistic details of disease progression. This mutation, which is associated with a mild form of metachromatic leukodystrophy (MLD), weakens the interaction between monomers, causing the biological assembly to favor the homo-dimer state over the homo-octamer state. **(c)** Clustering all SNPs that fall within a 5–10 Å vicinity of other mutations, we find that the largest cluster falls within 10 Å of both the metal-binding site and the substrate-binding site (residues 306 to 309 in PDB entry e2sp). These specific cases all cause a severe form of MLD in adults, juveniles, and infants. The distribution of structural and disease properties associated with all 76 SNPs that map to the representative domain of this protein (d1e2sp_) is given by the bar chart. The majority of cases map to the calcium binding domain, substrate binding domain, and have a significant effect on enzyme activity. **(d)** ARSA and its neighborhood of surrounding reactions link to a number of disease-associated mutations, indicating that this is a network hotspot for deleterious or potentially harmful mutations. In many cases, the proteins catalyzing these reactions also have available protein structural content (shown by a heat map and reaction link color), enabling 3D visualization of other SNPs in proteins in neighboring reactions. Figures for protein structures were generated using ChimeraX, the next-generation version of Chimera. Reactions are drawn with the minimal number of metabolites and cofactors for clarity.

Elucidating relationships between drug indications and their metabolic responses

Drug interventions influence the behavior of metabolic networks⁴², but the impact of drug treatment on metabolic responses and the mechanisms underlying these responses are poorly understood. We used Recon3D to combine large-scale data on drugs, their indications, and their effects on gene expression. These data were used to guide and inform genome-scale constraint-based modeling analyses^{42,43} to identify the metabolic pathways most perturbed in a given condition (**Supplementary Fig. 15**). More specifically, we used a machine-learning

approach to assess similarities in metabolic responses to a given drug (**Fig. 6a**). Using a genetic algorithm, the area under the curve (AUC) of the receiver operating characteristic (ROC) curve was maximized to predict the indication of the drug based on the type and degree of perturbation (**Fig. 6b**, **Supplementary Data 24** and **Supplementary Note 6**). Finally, we use the structural information in Recon3D to provide insights into the possible mechanisms by which the drugs exert their effects on metabolic pathways.

We first grouped 6,040 transcriptomic profiles (exposed to over 1,200 drug compounds in breast, leukemia, and prostate cancer cell

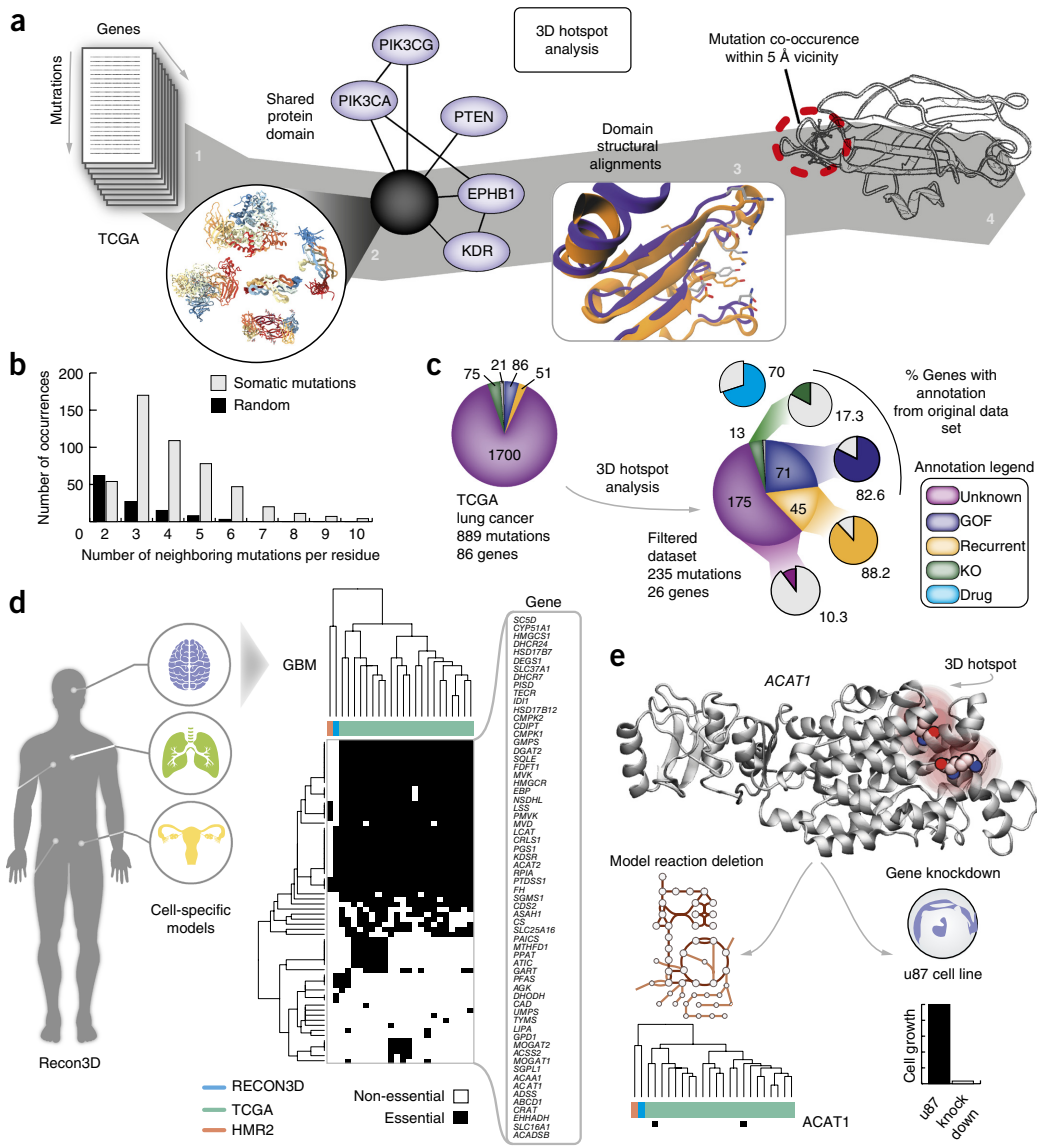


Figure 5 Protein structure-guided discovery of mutation hotspots across structurally related genes. Synchronization of protein structural domains, metabolic networks, and somatic mutation landscapes allows for stratification of variants into informative and meaningful sub-clusters. (a) The 3D hotspot analysis workflow. A list of genes with mutations³⁵ is cross-referenced with databases such as TCGA. In this example, we studied mutations taken from whole-exome sequence data from 178 tumor–normal pairs of lung squamous cell carcinoma³⁶. We then assembled protein structural information for this subset of genes with somatic mutations and evaluated the number of representative protein domains for this set of genes. In total, 86 genes associated with 889 missense mutations had available experimental crystallographic structures and could be linked to representative structural domains. We tallied the mutations occurring within 5 and 10 Å spheres for each representative domain. The domains with multiple mutations in a specific 3D location were termed “mutation hotspots.” (b) We compared the frequency of mutation co-occurrence (in a 5 Å sphere) in randomly selected residues (gray) within the same set of proteins with those taken from the lung cancer data set (black). This comparison strongly suggests that somatic mutations are more likely to be found neighboring other mutations than what is expected by chance ($P < 0.02$). (c) Selecting the top 25% of mutations (235/889) with the highest number of neighboring mutations (within the same 5 Å region in a representative protein domain) brings about a striking commonality that many are associated with known oncogenic roles. Information about various mutations was taken from several databases providing detailed annotations (which are color-coded in the plot), including recurrent sequence hotspots (R)¹², known oncogenes^{37,38} (<http://www.oncokb.org>), as well as drug (Olaparib/ BYL-719), Memorial Sloan Kettering level of evidence (3B), and other cancer subtype (endometrial/breast) associations (<http://www.mycancergenome.org>). For example, of all the mutations in this data set with gain-of-function (GOF) oncogenic associations, 83% are found in the subset of mutations selected for on the basis of 3D localization. Similarly high percentages are recovered for other characteristic annotations, including the frequency of occurrence (88%), association with endometrial cancer (100%), and association with breast cancer (40%). Intriguingly, percentage of mutations with unknown effects is greatly reduced from 90% in the total data set (bottom pie chart; 889 mutations across 86 genes) compared to 10% in the 3D filtered subset (top pie chart; 235 mutations across 26 genes). Random selection of 235 mutations (averaged across 10,000 trials) demonstrates that the probability of recovering the same percentage of mutations with known oncogenic roles is very low (shown by the white outlined bars). (d) We combined the 3D hotspot analysis with metabolic modeling and focused on the somatic landscape of glioblastoma multiforme⁵³. Gene knockdowns were performed in various models, including Recon3D, HMR2.0, and cell-specific (GBM) and patient-specific models. (e) The majority of models predicted ACAT1 to be non-essential. Yet, when analyzing the mutations in this gene in 3D, we find a mutation hotspot. The importance of this gene is further confirmed by experiment, demonstrating its importance to GBM growth⁴⁰. This example suggests that protein structure could facilitate model predictions by highlighting genes of interest using complementary information.

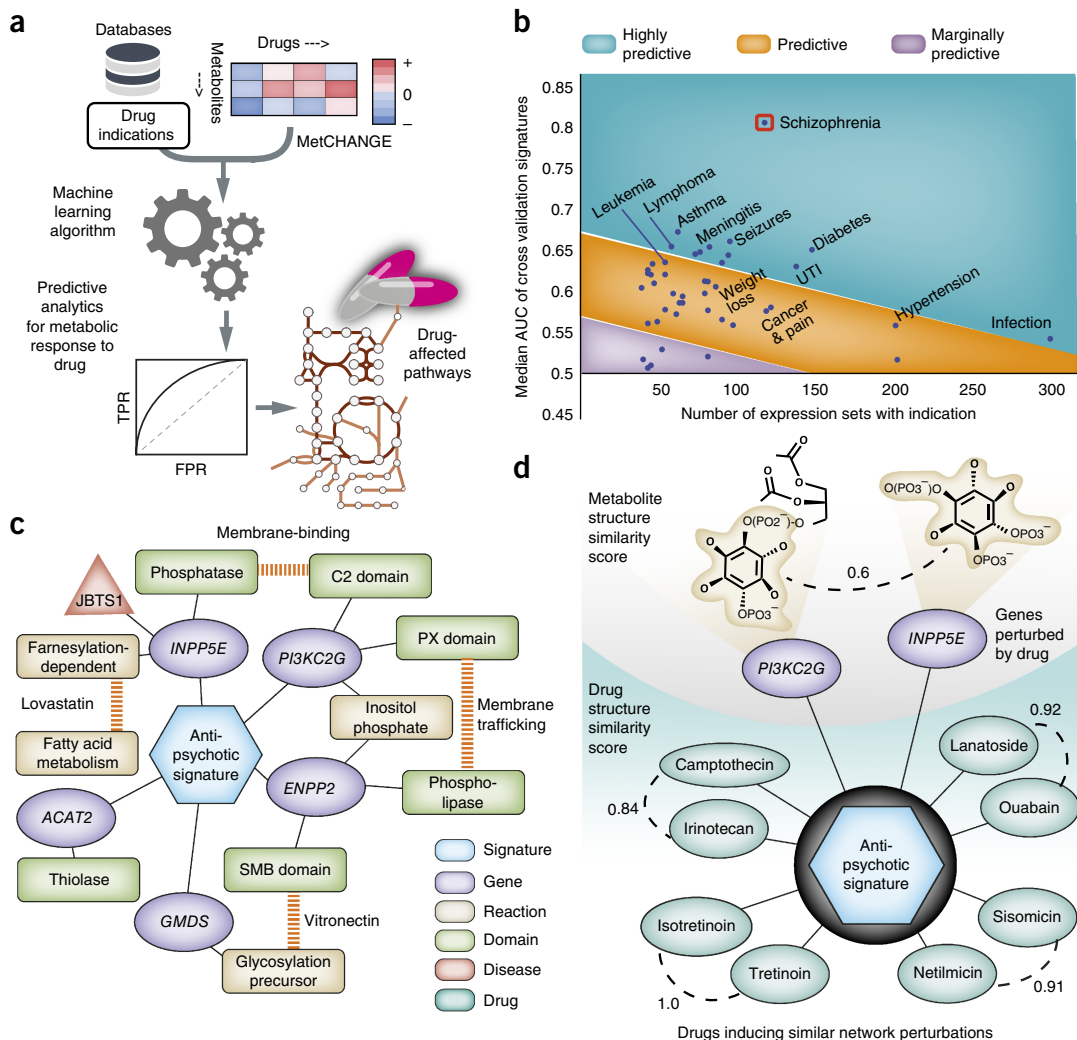


Figure 6 Identification of metabolic signatures linked to drug indications. **(a)** A machine-learning-based approach to predict metabolic responses to drugs. Drug indications were taken from the Side Effect Resource (SIDER) database⁴⁵ for all available drugs overlapping with drug-treated gene expression profiles from the Connectivity Map (CMap) database⁴⁴. A total of 47 drug indications were analyzed in the context of the metabolic network, based upon 1,459 expression sets from cell culture responses to 334 drugs (**Supplementary Data 26**). Using a genetic algorithm, the area under the curve (AUC) of the receiver operating characteristic (ROC) curve (e.g., comparing true positive rate, TPR, and false positive rate, FPR) was maximized to predict the indication of the drug based on the type and degree of perturbation. **(b)** Cross-validation results of metabolic gene expression signatures trained against drug indications versus the number of expression sets with the indication used in training. Results were empirically grouped as highly predictive, predictive, and marginally or poorly predictive based on AUC. Results were plotted with consideration to data set size, showing that the signature is conserved over a greater number of drugs and amount of noise. Schizophrenia appeared as a clear outlier with greater predictability for a relatively large number of expression sets and drugs (13 drugs used in training), indicating that the gene signature is highly conserved (median AUC of 0.8). **(c)** Analysis of the antipsychotic signature in the context of known metabolic effects in schizophrenia and antipsychotic therapy. Genes that cluster based on the antipsychotic drug indication signature are linked to structure, biochemical, and disease properties through Recon3D. Such connectivity networks provide a first glimpse at whether genes share similar biological functions or domain archetypes. **(d)** Perturbations in genes that cluster based on metabolite/drug similarity. Computing structural alignments of the drugs inducing the antipsychotic drug indication signature indicates that certain pairs are likely to have similar bioactivities (based on the Tanimoto coefficient > 0.8). Chemically similar drugs cluster into four structurally distinct groups that differ on the basis of drug class. Drugs within these four groups all induce the same drug indication signature despite being radically different in structure (Tanimoto coefficient < 0.2).

lines from the Connectivity Map, or CMap⁴⁴) by drug indication, using information from the Side Effect Resource (SIDER) database⁴⁵ (**Supplementary Table 7**). A total of 47 drug indications were analyzed in the context of the metabolic network, using a previously described machine-learning approach⁴² (**Supplementary Fig. 15**). The analysis revealed that indication-specific drugs induced similar patterns of gene expression changes or ‘gene indication signatures’. Our findings suggest that metabolic responses are significantly conserved for a wide range of drugs (**Fig. 6b**), with the most conserved pathway perturbations

occurring for antipsychotic drugs (median AUC of 0.80; **Supplementary Data 25**). For this specific case, the gene indication signature is composed of nine genes that have been previously associated with schizophrenia (**Supplementary Table 8**). We also find associations between changes in lipid and cholesterol pathways and common antipsychotic drug side effects (weight gain, cardiovascular risk, and anti-inflammatory effects). Notably, some drugs with entirely different indications shared similar pathway-level changes with antipsychotic drugs and had previously been tested as adjunctive schizophrenia treatments⁴⁶

(**Supplementary Table 9**). A list of the drugs with the most predictable metabolic responses is provided in **Supplementary Data 26**.

We then used protein and metabolite structural data in Recon3D to probe for mechanistic insights into drug response. In general, understanding mechanistic details entails identifying single or multiple targets of drug binding (or off-target binding) and the respective downstream effects. Information in Recon3D can be visualized as a topological network to indicate shared features across nodes (genes) in a gene indication signature. Displayed in **Figure 6c** is one connected hub of genes (antipsychotic gene indication signature) and several features for comparison: protein structural domains, metabolites, biochemical reactions, and disease relevance. For this signature, we found several overlapping features, such as the metabolic subsystems targeted by known drugs (e.g., lovastatin and fatty acid metabolism) and the function of certain protein domains (e.g., an influence in membrane binding/trafficking). Despite these shared domain functions, minimal structural alignment of the protein domains and metabolites indicates that the majority of genes in this signature are not direct drug targets, but may play a role in compensatory signaling pathways that mediate drug effects synergistically. Finally, structural alignment of the drug compounds themselves yielded unexpected results; drugs that induced the same pattern of perturbation (both drugs with known antipsychotic action and unrelated drug indications) were found to be structurally diverse (**Fig. 6d**). This finding is surprising given that drug discovery efforts tend to emphasize small changes in molecular structure to tune a desired biochemical effect. Here, we find that structurally diverse molecules exert similar effects on metabolic pathways, highlighting the potential of Recon3D for drug repurposing and the design of multitargeted therapies that support a new polypharmacological paradigm in drug research^{47,48}.

DISCUSSION

Recon3D is the first network reconstruction to include protein and metabolite structures as well as atom–atom mappings. Recon3D provides functional insights into genetic variation and the mechanisms underlying the effects of drugs on metabolic response in humans. It also serves as a computable knowledge-base with clear functional connectivity between genes and biochemical pathways. Pairing Recon3D with biomedical data provides a compelling avenue for studying disease at scale.

Recon3D integrates multiple layers of biological data and provides a tool to study variation and its impact on individual proteins and complex pathways. The inclusion of different data types offers new opportunities for network reconstruction in that it introduces atomic-scale properties, such as ligand-binding interactions; it provides new avenues for precision medicine by exploring human variation^{14,15}; and it enables the probing of genetic variation via changes in the molecular properties of proteins²⁰. In this way, individual sequence variations can be explicitly represented and the functional connections among disease, genetic perturbation, and drug action can be probed systematically.

Recon3D enables straightforward data integration, as its content has been linked to external databases (KEGG, PDB, CHEBI, PharmGKB, UniProt). This knowledge-base can be converted into a genome-scale model, which can be computationally interrogated and characterized. Constraint-based methods⁴³ can be used to assess network properties, and bioinformatics tools³² can be used to assess protein or metabolite properties. Our findings present preliminary, yet compelling, support for the potential of Recon3D to complement traditional structure-based approaches for empowering applications in drug discovery and target validation. We have shown that a systematic exploration of mutations in the context of their 3D spatial relationship provides a unique means for filtering out functionally relevant mutations and

determining potential genes of interest. Furthermore, analysis of *in vitro* drug-treated gene expression profiling in the context of the human metabolic network provides insight into the broad metabolic response to different drug therapies.

Recon3D provides a framework for integrating structure–function relationships and assessing specific and proteome-wide effects of sequence variation. Integrated frameworks like Recon3D enable understanding of how mutations or binding events lead to downstream responses and could aid in the identification of novel targets when coupled to structural bioinformatics¹⁶, molecular dynamics simulations^{20,49}, and kinetic modeling⁵⁰. In contrast, current metabolic models are not able to contextualize the effect of a sequence variant (beyond gene deletions) and therefore cannot be used to study disease-relevant mutations. Recon3D will potentially aid in translating biomedical knowledge, from large-scale omics data to drug discovery, target identification, and clinical biomarker development. Future efforts are likely to extend to precision medicine applications where drug responses can be assessed in the context of individual patient-specific genomes. Recon3D is available via two databases^{3,51} (<http://bigg.ucsd.edu/> and <http://vmh.life>).

METHODS

Methods, including statements of data availability and any associated accession codes and references, are available in the [online version of the paper](#).

Note: Any Supplementary Information and Source Data files are available in the online version of the paper.

ACKNOWLEDGMENTS

The results here are in whole or part based upon data generated by the TCGA Research Network: <http://cancergenome.nih.gov/>. This work was funded by the Novo Nordisk Foundation Center for Biosustainability and the Technical University of Denmark (grant number NNF10CC1016517), the National Institutes of Health (grant GM057089 to B.O.P.) and by the Luxembourg National Research Fund (FNR) through the National Centre of Excellence in Research (NCER) on Parkinson's disease and the ATTRACT programme (FNR/A12/01), by the European Union's Horizon 2020 research and innovation programme under grant agreement No 668738, by the Institutional Strategy of the University of Tübingen (German Research Foundation DFG, ZUK 63), and by Google Inc. (Summer of Code 2016). RCSB PDB is funded by the National Science Foundation (NSF DBI-1338415 to S.K.B.), the Department of Energy, and the National Institutes of Health (NIGMS and NCI). This research used resources of the National Energy Research Scientific Computing Center. The authors gratefully acknowledge P. Mischel and W. Zheng for experimental help and discussions on GBM, N. Lewis, A. McCammon, J. Mesirov, J.M. Thornton, J. Monk, and J. Lerman for scientific discussions and Z. King for help with Escher integration in RCSB PDB, M. Abrams for manuscript editing, V. Kohler and A.E. Kärcher-Dräger for drawing the platelet and RBC map in Escher, and F. Monteiro and M.A.P. Oliveira for help in reconstructing the dopamine subsystem.

AUTHOR CONTRIBUTIONS

Conceptualization: E.B., I.T., and D.C.Z.; methodology, reconstruction of metabolic network: S.S., I.T., R.M.T.F., A.D.D., A.H., and M.K.A.; reconstruction of GEM-PRO: E.B., N.M., and A.S.; 3D-hotspot analysis: E.B., A.P., A.S., and P.W.R.; machine learning: D.C.Z.; PDB visualization: A.A., A.P., A.D., R.M.T.F., and S.K.B.; atom–atom mapping: G.A.P.G. and R.M.T.F.; model testing and validation: I.T., R.M.T.F., S.S., M.K.A., D.C.Z., A.N., and F.G.; cell-specific and infant model simulations: M.K.A., A.N., and F.G.); investigation, E.B., D.C.Z., and G.A.P.G.; writing, original draft: E.B. and B.O.P.; writing, review and editing: all authors; funding acquisition: I.T., R.M.T.F., S.K.B., J.N., and B.O.P.; resources, I.T., R.M.T.F., S.K.B., J.N., and B.O.P.; supervision: I.T., R.M.T.F., S.K.B., and B.O.P.

COMPETING FINANCIAL INTERESTS

The authors declare no competing financial interests.

Reprints and permissions information is available online at <http://www.nature.com/reprints/index.html>. Publisher's note: Springer Nature remains neutral with regard to jurisdictional claims in published maps and institutional affiliations.

1. Bui, A.A.T. & Van Horn, J.D. Envisioning the future of 'big data' biomedicine. *J. Biomed. Inform.* **69**, 115–117 (2017).
2. O'Brien, E.J., Monk, J.M. & Palsson, B.O. Using genome-scale models to predict biological capabilities. *Cell* **161**, 971–987 (2015).
3. Thiele, I. *et al.* A community-driven global reconstruction of human metabolism. *Nat. Biotechnol.* **31**, 419–425 (2013).
4. Duarte, N.C. *et al.* Global reconstruction of the human metabolic network based on genomic and bibliomic data. *Proc. Natl. Acad. Sci. USA* **104**, 1777–1782 (2007).
5. Swainston, N. *et al.* Recon 2.2: from reconstruction to model of human metabolism. *Metabolomics* **12**, 109 (2016).
6. Pornputtапong, N., Nookaew, I. & Nielsen, J. Human metabolic atlas: an online resource for human metabolism. *Database* **2015**, bav068 (2015).
7. Argmann, C.A., Houten, S.M., Zhu, J. & Schadt, E.E. A next generation multiscale view of inborn errors of metabolism. *Cell Metab.* **23**, 13–26 (2016).
8. Gatto, F. & Nielsen, J. Pan-cancer analysis of the metabolic reaction network. Preprint at *bioRxiv* <https://www.biorxiv.org/content/early/2016/05/17/050187> (2016).
9. Ji, B. & Nielsen, J. New insight into the gut microbiome through metagenomics. *Adv. Genomics Genet.* **5**, 77–91 (2015).
10. Heinken, A. & Thiele, I. Systems biology of host-microbe metabolomics. *Wiley Interdiscip. Rev. Syst. Biol. Med.* **7**, 195–219 (2015).
11. Thiele, I. & Palsson, B.Ø. A protocol for generating a high-quality genome-scale metabolic reconstruction. *Nat. Protoc.* **5**, 93–121 (2010).
12. Chang, M.T. *et al.* Identifying recurrent mutations in cancer reveals widespread lineage diversity and mutational specificity. *Nat. Biotechnol.* **34**, 155–163 (2016).
13. Miller, M.L. *et al.* Pan-cancer analysis of mutation hotspots in protein domains. *Cell Syst.* **1**, 197–209 (2015).
14. Laskowski, R.A. *et al.* Integrating population variation and protein structural analysis to improve clinical interpretation of missense variation: application to the WD40 domain. *Hum. Mol. Genet.* **25**, 927–935 (2016).
15. Niu, B. *et al.* Protein-structure-guided discovery of functional mutations across 19 cancer types. *Nat. Genet.* **48**, 827–837 (2016).
16. Zhao, Z., Xie, L., Xie, L. & Bourne, P.E. Delineation of polypharmacology across the human structural kinome using a functional site interaction fingerprint approach. *J. Med. Chem.* **59**, 4326–4341 (2016).
17. Porta-Pardo, E. & Godzik, A. Mutation drivers of immunological responses to cancer. *Cancer Immunol. Res.* **4**, 789–798 (2016).
18. Rost, B. Twilight zone of protein sequence alignments. *Protein Eng.* **12**, 85–94 (1999).
19. Ebrahim, A. *et al.* Multi-omic data integration enables discovery of hidden biological regularities. *Nat. Commun.* (2016).
20. Mih, N., Brunk, E., Bordbar, A. & Palsson, B.O. A multi-scale computational platform to mechanistically assess the effect of genetic variation on drug responses in human erythrocyte metabolism. *PLOS Comput. Biol.* **12**, e1005039 (2016).
21. Mardinoglu, A. *et al.* Genome-scale metabolic modelling of hepatocytes reveals serine deficiency in patients with non-alcoholic fatty liver disease. *Nat. Commun.* **5**, 3083 (2014).
22. Sahoo, S., Haraldsdóttir, H.S., Fleming, R.M.T. & Thiele, I. Modeling the effects of commonly used drugs on human metabolism. *FEBS J.* **282**, 297–317 (2015).
23. Sahoo, S., Aurich, M.K., Jonsson, J.J. & Thiele, I. Membrane transporters in a human genome-scale metabolic knowledgebase and their implications for disease. *Front. Physiol.* **5**, 91 (2014).
24. Famiglietti, M.L. *et al.* Genetic variations and diseases in UniProtKB/Swiss-Prot: the ins and outs of expert manual curation. *Hum. Mutat.* **35**, 927–935 (2014).
25. Nilsson, A., Mardinoglu, A. & Nielsen, J. Predicting growth of the healthy infant using a genome scale metabolic model. *NPJ Syst. Biol. Appl.* **3**, 3 (2017).
26. Brunk, E. *et al.* Systems biology of the structural proteome. *BMC Syst. Biol.* **10**, 26 (2016).
27. Berman, J.H.M. *et al.* The protein data bank. *Nucleic Acids Res.* **106**, 16972–16977 (2000).
28. Preciat Gonzalez, G.A. *et al.* Comparative evaluation of atom mapping algorithms for balanced metabolic reactions: application to Recon3D. *J. Cheminform.* **9**, 39 (2017).
29. Noronha, A. *et al.* ReconMap: an interactive visualization of human metabolism. *Bioinformatics* **33**, 605–607 (2017).
30. Sherry, S.T. *et al.* dbSNP: the NCBI database of genetic variation. *Nucleic Acids Res.* **29**, 308–311 (2001).
31. Whirl-Carrillo, M. *et al.* Pharmacogenomics knowledge for personalized medicine. *Clin. Pharmacol. Ther.* **92**, 414–417 (2012).
32. Ye, Y. & Godzik, A. Flexible structure alignment by chaining aligned fragment pairs allowing twists. *Bioinformatics* **19** (Suppl. 2), ii246–ii255 (2003).
33. Kris, M.G. *et al.* Efficacy of gefitinib, an inhibitor of the epidermal growth factor receptor tyrosine kinase, in symptomatic patients with non-small cell lung cancer: a randomized trial. *J. Am. Med. Assoc.* **290**, 2149–2158 (2003).
34. von Bülow, R. *et al.* Defective oligomerization of arylsulfatase a as a cause of its instability in lysosomes and metachromatic leukodystrophy. *J. Biol. Chem.* **277**, 9455–9461 (2002).
35. Lawrence, M.S. *et al.* Mutational heterogeneity in cancer and the search for new cancer-associated genes. *Nature* **499**, 214–218 (2013).
36. Cancer Genome Atlas Research Network. Comprehensive genomic characterization of squamous cell lung cancers. *Nature* **489**, 519–525 (2012).
37. Gao, J. *et al.* Integrative analysis of complex cancer genomics and clinical profiles using the cBioPortal. *Sci. Signal.* **6**, p1 (2013).
38. Cerami, E. *et al.* The cBio cancer genomics portal: an open platform for exploring multidimensional cancer genomics data. *Cancer Discov.* **2**, 401–404 (2012).
39. Villa, G.R. *et al.* An LXR-cholesterol axis creates a metabolic co-dependency for brain cancers. *Cancer Cell* **30**, 683–693 (2016).
40. Geng, F. *et al.* Inhibition of SOAT1 suppresses glioblastoma growth via blocking SREBP-1-mediated lipogenesis. *Clin. Cancer Res.* **22**, 5337–5348 (2016).
41. Adzhubei, I., Jordan, D.M. & Sunyaev, S.R. Predicting functional effect of human missense mutations using PolyPhen-2. *Curr. Protoc. Hum. Genet.* **7**, 7.20 (2013).
42. Zielinski, D.C. *et al.* Pharmacogenomic and clinical data link non-pharmacokinetic metabolic dysregulation to drug side effect pathogenesis. *Nat. Commun.* **6**, 7101 (2015).
43. Orth, J.D., Thiele, I. & Palsson, B.Ø. What is flux balance analysis? *Nat. Biotechnol.* **28**, 245–248 (2010).
44. Lamb, J. *et al.* The Connectivity Map: using gene-expression signatures to connect small molecules, genes, and disease. *Science* **313**, 1929–1935 (2006).
45. Kuhn, M., Campillos, M., Letunic, I., Jensen, L.J. & Bork, P. A side effect resource to capture phenotypic effects of drugs. *Mol. Syst. Biol.* **6**, 343 (2010).
46. Fischer, A., Sananbenesi, F., Mungenast, A. & Tsai, L.-H. Targeting the correct HDACs to treat cognitive disorders. *Trends Pharmacol. Sci.* **31**, 605–617 (2010).
47. Xie, L., Xie, L., Kinnings, S.L. & Bourne, P.E. Novel computational approaches to polypharmacology as a means to define responses to individual drugs. *Annu. Rev. Pharmacol. Toxicol.* **52**, 361–379 (2012).
48. Hopkins, A.L. Network pharmacology. *Nat. Biotechnol.* **25**, 1110–1111 (2007).
49. Brunk, E. & Rothlisberger, U. Mixed quantum mechanical/molecular mechanical molecular dynamics simulations of biological systems in ground and electronically excited states. *Chem. Rev.* **115**, 6217–6263 (2015).
50. Bordbar, A. *et al.* Personalized whole-cell kinetic models of metabolism for discovery in genomics and pharmacodynamics. *Cell Syst.* **1**, 283–292 (2015).
51. King, Z.A. *et al.* BiGG Models: a platform for integrating, standardizing and sharing genome-scale models. *Nucleic Acids Res.* **44** D1, D515–D522 (2016).
52. Hastings, J. *et al.* The ChEBI reference database and ontology for biologically relevant chemistry: enhancements for 2013. *Nucleic Acids Res.* **41**, D456–D463 (2013).
53. Brennan, C.W. *et al.* The somatic genomic landscape of glioblastoma. *Cell* **155**, 462–477 (2013).

ONLINE METHODS

Metabolic reconstruction. Recon3D has been assembled using multiple data sources, that is, HMR 2.00 (ref. 6) (2,478 reactions), metabolomics data sets (1,865 reactions), a drug module²² (721 reactions), a transport module (51 reactions), host–microbe reactions (24 reactions), absorption and metabolism of dietary compounds (20 reactions), and others (1,004 reactions). The ‘others’ category included reactions that captured metabolism in specific human organs, (e.g., kidney), as well as novel metabolic pathways of lipoproteins, bile acids, and sphingolipids. The expansion of Recon 2 was performed in an iterative manner (**Supplementary Fig. 1**). With each addition, there followed extensive model debugging and manual curation for flux consistency and refinement.

Recon 2 was expanded in two stages: (i) additions of new reactions and (ii) network refinements for building a high-quality flux-consistent model (**Supplementary Fig. 1**). The total number of novel additions included 6,163 reactions, 1,589 metabolites, and 1,654 genes completing Recon3D. These new reactions were mostly from transport (32%), lipid metabolism (24%), exchange (19%), xenobiotic (11%), and amino acid (7%) metabolism (**Supplementary Fig. 2b,c**). Other major additions include those required for debugging the network for flux consistency (10% of newly added reactions), reactions representing organ-specific metabolism (7%), transport module (2% of newly added reactions), and those representing lipoprotein metabolism (2% of newly added reactions), novel dietary compounds and their associated reactions (1% of newly added reactions), and reactions capturing interaction between gut microbes and host (1% of newly added reactions). For details on the precise metabolic pathways, see **Supplementary Note 1**.

The largest contribution for new metabolic genes were those from: (i) lipid metabolism (10%), (ii) carbohydrate metabolism (5%), (iii) transport processes (5%), (iv) amino acid (3%), and (v) nucleotide metabolism and vitamin metabolism (1%) (**Supplementary Fig. 2**). The miscellaneous category mostly contained genes from HMR 2.0 (99%) (**Supplementary Fig. 2**). The largest contribution for new metabolites were lipid (42%) and amino acid (19%) classes. Novel metabolites added in other subsystems include miscellaneous and xenobiotics (18%), carbohydrates (2%), vitamins (1.4%), and nucleotide (0.3%) metabolism (**Supplementary Fig. 2**).

Once reactions and genes were added to Recon3D, the reconstruction was subjected to various quality control or quality assurance tests (**Supplementary Fig. 1**). These included (i) checking for reaction and metabolite duplicity, (ii) modification of gene–protein–reaction associations, (iii) modification of metabolite formulae to pH 7.2 along with mass-charge balancing of reactions, (iv) a leak test, checking for stoichiometric and flux consistency and checking for thermodynamic feasibility⁵⁴, (v) debugging and curation for removal of dead-end metabolites, and (vi) checking for network accomplishment of defined functions/tests (**Supplementary Fig. 1**).

To check reaction and metabolite duplicity, we took several approaches. First, Quek *et al.*⁵⁵ reported 95 duplicate metabolites, 71 of which were replaced (**Supplementary Data 9** and **Supplementary Note 1**). Second, the reaction and metabolite duplicity was checked for HMR reactions and metabolites (before inclusion in Recon 3). The metabolite formulae, particularly those received from HMR 2.0, were adjusted to an internal pH of 7.2, using mol files²⁸ and COBRA toolbox⁵⁶ and ChemAxon software (<https://chemicalize.com/>). This led to correct assignment of reaction stoichiometry and mass-charge-balancing of reactions. Third, gene–protein–reaction associations were curated and corrected for 2,180 reactions (**Supplementary Data 6** and **7** and **Supplementary Note 1**). Finally, we performed additional QC/QA tests (e.g., functional leaks, production of matter from water and oxygen, etc.).

The COBRA toolbox⁵⁶ was used to identify a subset of 10,600 reactions involving 5,835 metabolites, representing the stoichiometrically consistent flux balance model. The final model was tested for 431 model objectives, representing essential biochemical functions of the human body. The model debugging was mostly done by the addition of extracellular and intracellular transport reactions. Examples include the addition of novel transport proteins for bile acids and folate intermediates. Novel intracellular transport proteins, i.e., mitochondrial pyruvate carriers (*MPC1*, GeneID: 51660 and *MPC2*, GeneID: 25874) were added for phenylpyruvate that operates in a proton symport mechanism⁵⁷. These transport reactions connected the intracellular

and extracellular compartments of the model, enabling flux consistency. Manual curation of the relevant scientific literature was followed to obtain complete information on the respective biochemical pathway. A typical example includes the addition of 4-methyl-thio-oxo-butyrate (an intermediate of methionine metabolism) into the network. Upon literature curation, addition of the alternative route of methionine transamination and decarboxylation reactions were identified and added (**Supplementary Data 1**).

Please refer to **Supplementary Note 1** and **Supplementary Data 1–10** for detailed information on the network building and refinements.

GEM-PRO reconstruction. We followed the previously described procedure²⁶ to map, assess, and refine PDB or homology models for integration into genome-scale models. For Recon3D, additions to the gene identifier mapping workflow were made to address inconsistencies in gene isoforms across database entries and the ability to link isoforms to available homology models. In addition, QC/QA steps were taken in order to ensure the correct sequence was being retrieved (**Supplementary Fig. 5** and **Supplementary Note 3**). For PDB structures with missing residues, we have filled in the gaps by querying previously generated databases of I-TASSER homology models^{58,59}, and manually generating homology models for genes that were not part of these databases using previously defined protocols^{26,60}. In the final master GEM-PRO data frame (**Supplementary Data 11**), we note where available homology models have been mapped to their respective genes. For most homology modeling procedures, the amino acid sequence of a protein is all that is required to generate a homology model of a protein. It is important to note that for certain PDB structures with unresolved residues or gaps in the structure a homology model can also be generated to enhance the structural coverage of the amino acid sequence. Homology models were not generated for any sequences longer than 600 amino acids long. We assessed the overall quality of the information coming from homologous templates in terms of (i) which organism the protein was crystallized from, (ii) the resolution of the PDB template, and (iii) the deposition date. We used these properties to compare the templates that were used to construct homology models in the previous GEM-PRO models with those of the recently updated versions (**Supplementary Tables 2–4** and **Supplementary Fig. 6**).

To identify structures for the given set of metabolites in Recon3D, we evaluated a number of databases where metabolite structures are publicly available, such as PDB (ligand-expo: <http://ligand-expo.rcsb.org/>, <http://ligand-expo.rcsb.org/ld-search.html>), PubChem⁶¹ (<https://pubchem.ncbi.nlm.nih.gov/>), and ChEBI (<http://www.ebi.ac.uk/chebi/>). We downloaded structures in various formats: 2D structure in .mol format (ChEBI), 3D structure in .sdf format (PubChem⁶¹), and in .pdb/.xyz format (RCSB). **Supplementary Data 14** provides all the information content processed for metabolites in Recon3D, which includes SMILES and INCHI descriptors, Kyoto Encyclopedia of Genes and Genomes (KEGG)⁶² IDs, CID IDs, CID file names, ChEBI file names, ChEBI IDs, and experimental coordinate file URL locations and the ideal coordinate file name. The ChEBI mapping procedure contained the following steps: (i) identification of the particular metabolite from ChEBI using the source link (the metabolite name was the starting point of search which is taken from the metabolite names in the **Supplementary Data 14**); (ii) checking the molecular formula and charge (neutral or charged) of the metabolite in the ChEBI database; (iii) capturing the ChEBI link, ChEBI ID, SMILES, and INCHI into the respective fields in the data set spreadsheet; (iv) 2D-structure is downloaded in .mol format. The same overall search was conducted in PubChem and PDB (Ligand expo) with slight variations as to the initial search inputs and file type outputs.

The data set of human single nucleotide polymorphisms (SNPs) and single nucleotide variants (SNVs) was collected from UniProt from a subset of protein altering variants from the 1000 Genomes Project. Furthermore, all SNPs and SNVs for model genes were downloaded directly from dbSNP (<http://www.ncbi.nlm.nih.gov/SNP/>) via the Ensembl BioMart interface⁶³. We then selected all variants that were characterized to be ‘damaging’ or ‘possibly damaging’ as a predicted functional impact using the PolyPhen2 bioinformatics tool⁴¹. Functional annotations of the missense mutations were also annotated using SIFT (<http://sift.jcvi.org/>). In addition, we linked the missense variants to their gene–drug associations (clinically relevant pharmacogenomics interactions) using the PharmGKB pharmacogenomics database (<https://www.pharmgkb.org/>). All annotated gene–drug pairs contain information

such as dosing guidelines, drug label annotations and each pair is generally specified in more than 1 type of annotation (dosing guideline, drug label, clinical annotation, variant annotation, VIP, or pathway). These selected pharmacogenomic associations allow us to understand whether certain missense variants have functional effects on drug therapies. All selected missense variants and their drug associations have been provided as **Supplementary Data 15** and **16**.

More details on the process and procedure for network reconstruction, protein and metabolite structure integration, identification of representative protein domains, linking to pharmacogenomics databases, linking to cancer genome atlases, mutation hotspot analyses, and comparison of tissue-specific cancer and pharmacogenomic/gene variation networks are all provided in **Supplementary Notes 3** and **4**.

Atom–atom mapping. Generation of atom mapping data requires chemical structures, reaction stoichiometry and an atom mapping algorithm. Atom mappings were predicted using the Reaction Decoder Tool⁶⁴, and the DREAM algorithm⁶⁵ for 7,535 (86%) mass balanced reactions with implicit and explicit hydrogens, respectively, while Reaction Decoder Tool and the CLCA algorithm⁶⁶ were used to predict atom mappings for a further 269 reactions with incompletely specified metabolites (e.g., R group) with implicit and explicit hydrogens, respectively. We compared these predictions for internal reactions to a set of 512 reactions with atom mappings that we and others manually curated (**Supplementary Note 3**). This reaction set is representative of all six top-level (Enzyme Commission) EC numbers. Based on this comparison, we observed that the predicted atom mappings are highly accurate for most of the reaction types²⁸ (**Supplementary Fig. 7**).

3D mutation hotspot analysis. We filtered a set of mutations (whose genes are associated with experimental protein structures) based on whether the location of the mutated residue itself was resolved (e.g., certain protein domains are unresolved due to flexibility or unstructured regions of the protein being challenging to crystallize). Once the subset of mutations was established to (i) be linked to genes with experimental protein structures and (ii) be located within regions of the protein that were experimentally determined, we carried out 3D structure alignments between all proteins and their representative domains (mapping to representative protein domains is described previously in the section entitled “mapping and alignment of PDBs to their representative domains”). In contrast to sequence alignments, 3D structure alignments find a best fit in terms of the 3D shape or geometry of two proteins. Therefore, any two proteins that have different sequences but share a common domain architecture can be successfully aligned in 3D space. Similar to sequence alignments, the 3D structural alignment provides a direct residue-to-residue mapping for residues that share structurally equivalent positions in a common/shared domain motif. Once this residue-to-residue mapping was established for all proteins in our data set, we located 3D “hotspot” mutations by tallying all residues in the representative domains that map to mutated residues in a given protein of interest. To this end, certain residues in a representative domain may have multiple hits if more than one gene is linked to that representative domain and the same structurally equivalent residue is mutated across various genes. **Supplementary Data 17** provides the mapping between the residue number of the Uniprot missense variant > the PDB residue number > the PDB chain where the residue is located > the representative domain ID linked to a given PDB chain > the structurally equivalent residue within that representative domain.

Mapping cancer mutations in 3D. We used the TCGA level 3 variant data in the cBioPortal (<http://www.cbioperl.org/>). For this study, we used high-level (processed) data from a subset of pre-analyzed mutations from 178 tumor-normal pairs of lung squamous cell carcinoma³⁶. When the MutSig1.0 approach was applied on this data set³⁵, it identified 450 genes as significantly mutated. Starting from this set of genes, we identified a subset of 86 genes that have Uniprot accession numbers and protein structural information. Within this set of genes, we found that 889 somatic cancer mutations map to residues that have been successfully resolved in the crystallographic structures of proteins. We used the list of 86 genes to query the cBioPortal web-based data set and downloaded various

information including: somatic cancer mutations, cancer study sample IDs, amino acid mutations, annotations (coming from various sources, such as <http://oncokb.org/> and <https://www.mycancergenome.org/>), type of mutation, copy number changes, overlapping mutations in COSMIC, the predicted functional impact score (from Mutation Assessor), variant allele frequency in the tumor sample, and total number of nonsynonymous mutations in the sample. A summary of cancer data sets used in this study is given in **Supplementary Data 21** and a detailed summary of all somatic mutations for this set of genes is provided in **Supplementary Data 22** and **23**. The 3D hotspot analysis was carried out as detailed above and mutations were rank-ordered on the basis of how many mutations fell within a 5 Å sphere (i.e., number of nearest neighbors). We performed a sensitivity analysis to understand whether the selection of data points had an effect on the significance of these results.

The above 3D hotspot analysis approach was also applied to 22 genes from which cancer mutations have already been analyzed⁵³ (exome samples of 291 glioblastomas) and 92 genes involved in cholesterol metabolism, owing to the fact that cholesterol biosynthesis plays an important role in GBM³⁹.

Statistical tests. We performed a sensitivity analysis to understand whether the selection of data points had an effect on the significance of these results. We find that the 3D hotspot analysis is more likely to select somatic mutations compared to a random selection. Data points (50–700) were selected so that 0.065–0.91 of the total data set was covered. We performed the 3D hotspot analysis across the different selections and found *P* values in the range 0.017–0.049 compared to 0.182–0.241, using a random residue selection.

For annotations of mutations that are known oncogenes and known hotspots, selection of the databases on 3D hotspot analysis is important, regardless of the number of mutations (or % of data) selected (*P* < 0.05). Compared to a random selection, our computed (using a two-tailed *t*-test) *p* value is > 0.1. We also performed a sensitivity analysis using the slices of the total data set as mentioned above (50–500 data points) and computed the total number of known oncogenes and known hotspots (from previously published analyses), using the 3D hotspot analysis compared to a random selection. We find that the percentage of data selected is significantly higher using the 3D hotspot analysis. For known oncogenes, 37–83% of the data is selected using 3D hotspot compared to 0.046–0.43 at random. Similarly, for known hotspots, 72.5–88.3% of the data is selected using 3D hotspot analysis compared to 9.8–64%. See **Supplementary Note 5** for more information.

Gene deletion simulations in GBM. *In silico* single gene deletion (SGD) simulations were performed as previously described⁶⁷. Given a certain GEM, the simulation of a SGD was performed by formulating the linear program problem (1) for each gene *g* in the GEM:

- (1) $\max v_{obj}$ subject to:
- (2) $0 < v_{obj} < \gamma$
- (3) $\mathbf{S} \cdot \mathbf{v} = 0$
- (4) $-1000 \leq v_j \leq +1000 \forall j \in \{\text{Exchange reaction indexes for medium metabolites}\}$
- (5) $v_r = 0$ where $r \in \{\text{Reaction indexes univocally encoded by gene } g\}$

where v_{obj} is the flux through the biomass equation, γ is an arbitrary number set to 1, \mathbf{S} is the stoichiometric matrix of the GEM (that is, a $m \times n$ matrix where m is the number of metabolites and n is the number of reactions and each (i,j) entry is the stoichiometric coefficient of the metabolite corresponding to row *i* in the reaction corresponding to column *j*), \mathbf{v} is the vector containing the values of the fluxes through each reaction in the GEM, and *j* indexes each exchange reaction known to be present in a rich mammalian medium (Ham's medium, HAM; see **Supplementary Note 5** for more details). The simulation was carried out for the following GEMs: Recon3D, HMR2.00, and 22 personalized GEMs for glioblastoma multiforme (GBM) previously reconstructed using HMR2.00 as a template from as many GBM expression profiles retrieved at The Cancer Genome Atlas⁸.

Drug perturbation analysis. To compute metabolic pathways with gene expression perturbed by drugs, the human metabolic network model was first converted into an irreversible network. Then, the MetChange algorithm⁴² was run using gene expression presence/absence p-values from the Connectivity Map (Cmap) database⁴⁴ build 02. Drug indications were taken from the Side Effect Resource (SIDER) database⁴⁵ for all available drugs overlapping with the Cmap database. Synonyms were aggregated when present as with side effects. A minimum of ten drugs for each indication was required for the inclusion in the analysis, corresponding to a much greater number of expression sets for each indication. A total of 48 drug indications were analyzed for 1,459 expression sets corresponding to 334 drugs. A genetic algorithm (Supplementary Fig. 15) was then implemented as described in Supplementary Note 6. Details of the gene indication signatures can be found in Supplementary Note 6.

Code availability. “IndiFinder.m” contains the Matlab implementation of the genetic algorithm for finding metabolic signatures underlying drug indications given presence/absence of the indication existing for a given sample. It is submitted as **Supplementary Software** and requires previous installation of the COBRA Toolbox. Code is commented for guidance.

Life Sciences Reporting Summary. Further information on experimental design is available in the **Life Sciences Reporting Summary**.

Data availability. Recon3D is available as a metabolic reconstruction at <http://vmh.life>. A GIT repo that contains the GEMPRO, GBM-specific model files and simulations, and gene deletion simulations can be accessed via <https://github.com/SBRG/Recon3D>. Recon3D GEM-PRO has been consolidated into a shareable JSON file and submitted as **Supplementary Data 27**, which can be used to start structural analyses. This model assigns a single representative structure per gene in the reconstructed metabolic model. The accompanying software package required for reading and working with the GEM-PRO JSON is available at <https://github.com/SBRG/ssbio>. This entire repository can be cloned to a user’s computer and contains Jupyter notebooks in the root directory to guide a user through the content available in the Recon3D GEM-PRO model (Recon3D_GP - Loading and Exploring the GEM-PRO.ipynb) as well as to update the model with revised sequence information or newly deposited structures in the PDB (Recon3D_GP - Updating the GEM-PRO.ipynb). This

repository also includes all sequence and structure files mapped per gene, metadata downloaded through UniProt and the PDB, as well as the ability to rerun the QC/QA pipeline with different parameters such as sequence identity and resolution cutoffs. These notebooks also include basic visualization features enabled with the NGL viewer package⁶⁸.

54. Noor, E., Haraldsdóttir, H.S., Milo, R. & Fleming, R.M.T. Consistent estimation of Gibbs energy using component contributions. *PLOS Comput. Biol.* **9**, e1003098 (2013).
55. Quek, L.-E. *et al.* Reducing Recon 2 for steady-state flux analysis of HEK cell culture. *J. Biotechnol.* **184**, 172–178 (2014).
56. Heirendt, L. *et al.* Creation and analysis of biochemical constraint-based models: the COBRA Toolbox v3.0. Preprint at <https://arxiv.org/abs/1710.04038> (2017).
57. Dawson, P.A., Lan, T. & Rao, A. Bile acid transporters. *J. Lipid Res.* **50**, 2340–2357 (2009).
58. Xu, D. & Zhang, Y. Ab Initio structure prediction for *Escherichia coli*: towards genome-wide protein structure modeling and fold assignment. *Sci. Rep.* **3**, 1895 (2013).
59. Zhou, H., Gao, M., Kumar, N. & Skolnick, J. SUNPRO: Structure and function predictions of proteins from representative organisms <http://cssb.biology.gatech.edu/sunpro/index.html> (2012).
60. Roy, A., Kucukural, A. & Zhang, Y. I-TASSER: a unified platform for automated protein structure and function prediction. *Nat. Protoc.* **5**, 725–738 (2010).
61. Kim, S. *et al.* PubChem substance and compound databases. *Nucleic Acids Res.* **44** D1, D1202–D1213 (2016).
62. Kanehisa, M., Sato, Y., Kawashima, M., Furumichi, M. & Tanabe, M. KEGG as a reference resource for gene and protein annotation. *Nucleic Acids Res.* **44** D1, D457–D462 (2016).
63. Kinsella, R.J. *et al.* Ensembl BioMarts: a hub for data retrieval across taxonomic space. *Database* **2011**, bar030 (2011).
64. Rahman, S.A. *et al.* Reaction Decoder Tool (RDT): extracting features from chemical reactions. *Bioinformatics* **32**, 2065–2066 (2016).
65. First, E.L., Gounaris, C.E. & Floudas, C.A. Stereochemically consistent reaction mapping and identification of multiple reaction mechanisms through integer linear optimization. *J. Chem. Inf. Model.* **52**, 84–92 (2012).
66. Kumar, A. & Maranas, C.D. CLCA: maximum common molecular substructure queries within the MetRxn database. *J. Chem. Inf. Model.* **54**, 3417–3438 (2014).
67. Gatto, F., Miess, H., Schulze, A. & Nielsen, J. Flux balance analysis predicts essential genes in clear cell renal cell carcinoma metabolism. *Sci. Rep.* **5**, 10738 (2015).
68. Rose, A.S. & Hildebrand, P.W. NGL Viewer: a web application for molecular visualization. *Nucleic Acids Res.* **43** W1, W576–W579 (2015).

Life Sciences Reporting Summary

Nature Research wishes to improve the reproducibility of the work that we publish. This form is intended for publication with all accepted life science papers and provides structure for consistency and transparency in reporting. Every life science submission will use this form; some list items might not apply to an individual manuscript, but all fields must be completed for clarity.

For further information on the points included in this form, see [Reporting Life Sciences Research](#). For further information on Nature Research policies, including our [data availability policy](#), see [Authors & Referees](#) and the [Editorial Policy Checklist](#).

► Experimental design

1. Sample size

Describe how sample size was determined.

Sample size was chosen based on available data in TCGA for cancer type

2. Data exclusions

Describe any data exclusions.

No data was excluded from the analyses

3. Replication

Describe whether the experimental findings were reliably reproduced.

Replication was used in the ten-fold cross validation study and replication of trials for the 3D hotspot analysis was also used (10 times)

4. Randomization

Describe how samples/organisms/participants were allocated into experimental groups.

Yes, random trials (randomly chosen amino acid positions) were used to determine significance of finding mutations within 5 angstrom volume of other mutations in the same protein.

5. Blinding

Describe whether the investigators were blinded to group allocation during data collection and/or analysis.

Not relevant in this case since we are using data previously deposited and analyzed in TCGA

Note: all studies involving animals and/or human research participants must disclose whether blinding and randomization were used.

6. Statistical parameters

For all figures and tables that use statistical methods, confirm that the following items are present in relevant figure legends (or in the Methods section if additional space is needed).

n/a Confirmed

- The exact sample size (n) for each experimental group/condition, given as a discrete number and unit of measurement (animals, litters, cultures, etc.)
- A description of how samples were collected, noting whether measurements were taken from distinct samples or whether the same sample was measured repeatedly
- A statement indicating how many times each experiment was replicated
- The statistical test(s) used and whether they are one- or two-sided (note: only common tests should be described solely by name; more complex techniques should be described in the Methods section)
- A description of any assumptions or corrections, such as an adjustment for multiple comparisons
- The test results (e.g. P values) given as exact values whenever possible and with confidence intervals noted
- A clear description of statistics including central tendency (e.g. median, mean) and variation (e.g. standard deviation, interquartile range)
- Clearly defined error bars

See the web collection on [statistics for biologists](#) for further resources and guidance.

► Software

Policy information about [availability of computer code](#)

7. Software

Describe the software used to analyze the data in this study.

We use python modules (open source) and cobra matlab/cobrapy (open source) - we made simulation code available through github

For manuscripts utilizing custom algorithms or software that are central to the paper but not yet described in the published literature, software must be made available to editors and reviewers upon request. We strongly encourage code deposition in a community repository (e.g. GitHub). [Nature Methods guidance for providing algorithms and software for publication](#) provides further information on this topic.

► Materials and reagents

Policy information about [availability of materials](#)

8. Materials availability

Indicate whether there are restrictions on availability of unique materials or if these materials are only available for distribution by a for-profit company.

No restrictions

9. Antibodies

Describe the antibodies used and how they were validated for use in the system under study (i.e. assay and species).

irrelevant to experiments

10. Eukaryotic cell lines

a. State the source of each eukaryotic cell line used.

irrelevant to experiments

b. Describe the method of cell line authentication used.

irrelevant to experiments

c. Report whether the cell lines were tested for mycoplasma contamination.

irrelevant to experiments

d. If any of the cell lines used are listed in the database of commonly misidentified cell lines maintained by [ICLAC](#), provide a scientific rationale for their use.

irrelevant to experiments

► Animals and human research participants

Policy information about [studies involving animals](#); when reporting animal research, follow the [ARRIVE guidelines](#)

11. Description of research animals

Provide details on animals and/or animal-derived materials used in the study.

irrelevant to experiments

Policy information about [studies involving human research participants](#)

12. Description of human research participants

Describe the covariate-relevant population characteristics of the human research participants.

irrelevant to experiments